Published in final edited form as:

Proc SPIE Int Soc Opt Eng. 2022 ; 12034: . doi:10.1117/12.2611787.

Breast image registration for surgery: Insights on material mechanics modeling

Morgan J. Ringel[1,4], **Winona L. Richey**[1,4], **Jon Heiselman**[1,4], **Ma Luo**[1,4], **Ingrid M. Meszoely**[2], **Michael I. Miga**[1,3,4,5,6]

[1]Vanderbilt University, Department of Biomedical Engineering, Nashville, TN USA

[2]Vanderbilt University Medical Center, Division of Surgical Oncology, Nashville, TN USA

[3]Vanderbilt University Department of Radiology and Radiological Sciences, Nashville, TN USA

[4]Vanderbilt Institute for Surgery and Engineering, Nashville, TN USA

[5]Vanderbilt University Medical Center, Department of Neurological Surgery, Nashville, TN USA

[6]Vanderbilt University Medical Center, Department of Otolaryngology-Head and Neck Surgery, Nashville, TN USA

Abstract

Breast conserving surgery (BCS) is a common procedure for early-stage breast cancer patients. Supine preoperative magnetic resonance (MR) breast imaging for visualizing tumor location and extent, while not standard for procedural guidance, more closely represents the surgical presentation compared to conventional diagnostic pendant positioning. Optimal utilization for surgical guidance, however, requires a fast and accurate image-to-physical registration from preoperative imaging to intraoperative surgical presentation. In this study, three registration methods were investigated on healthy volunteers' breasts (n=11) with the arm-down position simulating preoperative imaging and arm-up position simulating intraoperative data. The registration methods included: (1) point-based rigid registration using synthetic fiducials, (2) non-rigid biomechanical model-based registration using sparse data, and (3) a data-dense 3D diffeomorphic image-based registration from the Advanced Normalization Tools (ANTs) repository. The average target registration errors (TRE) were 10.4 ± 2.3, 6.4 ± 1.5, and 2.8 ± 1.3 mm (mean ± standard deviation) and the average fiducial registration errors (FRE) were 7.8 ± 1.7, 2.5 ± 1.1, and 3.1 ± 1.1 mm (mean ± standard deviation) for the point-based rigid, nonrigid biomechanical, and ANTs registrations, respectively. Additionally, common mechanics-based deformation metrics (volume change and anisotropy) were calculated from the ANTs deformation field. The average metrics revealed anisotropic tissue behavior and a statistical difference in volume change between glandular and adipose tissue, suggesting that nonrigid modeling methods may be improved by incorporating material heterogeneity and anisotropy. Overall, registration accuracy significantly improved with increasingly flexible registration methods, which may inform future development of image guidance systems for lumpectomy procedures.

Keywords

breast cancer; lumpectomy; surgical guidance; registration; finite element modeling; deformable image registration

1. INTRODUCTION

Breast conserving surgery (BCS) is recommended for the majority of patients with early-stage breast cancer, and a successful surgical outcome depends on achieving negative tumor margins to prevent reoperation and the likelihood of recurrence[1]. Breast magnetic resonance (MR) imaging has high sensitivity and accuracy for tumor size estimation and has been used for preoperative planning of BCS procedures[2]. Additionally, MR imaging with the patient in the supine position has been shown to more closely represent tumor extent in surgery compared to prone positioning (breast pendant) which is subject to large gravity-induced deformations[3,4]. In recognition of this, the feasibility of using preoperative MR supine imaging combined with optical tracking and ultrasound imaging for assisting intraoperative navigation has been explored[5]. Going further, work on the use of intraoperative MR imaging to assist directly during the procedure by re-imaging has been investigated[6].

While direct re-imaging is an attractive option, the encumbrance and cost are likely to inhibit adoption. Using preoperatively acquired supine MR image volumes to guide lumpectomy procedures would be highly dependent on calculating an accurate 3D image-to-physical registration[7]. As suggested above, registration for BCS is particularly challenging since the preoperative and surgical presentations differ. Typically, supine MR imaging requires the arm to be either down or up to fit in a closed bore MRI scanner. In comparison, lumpectomy is typically performed with the ipsilateral arm extended laterally in a T-shape. When considering registration, rigid techniques are fast but fail to account for large soft-tissue deformations that occur from changes in position[8,9]. Non-rigid registration methods using biomechanical models can improve registration accuracy yet are non-trivial in implementation[10,11]. For example, developing biomechanical models that accurately capture large nonrigid breast deformations is challenging due to the variation in breast material properties and anatomical body forces[12]. It is also unclear how patient-specific ligament structure including suspensory Cooper’s ligaments and the superficial fascia may affect breast deformations[13].

One important aspect to consider with registration methods is the nature of the data that enables the process. Ultimately, both rigid and nonrigid registration methods depend on acquiring sparse geometric or intensity data in the intraoperative environment to establish correspondence between the preoperative image and intraoperative data. In the work reported here, supine MR imaging was acquired in an arm-down and arm-up presentation to represent preoperative and a mock intraoperative breast state. In some respect, this represents a more considerable challenge than the laterally extended (T-shape) arm positioning used in typical lumpectomy procedures. Nevertheless, this allowed for a ‘gold standard’ by providing full 3D volumetric visualization of the breast in a before- and after- deformation state. Image-to-image registration was utilized to provide a ‘best’ comparator of the volumetric transformation. Additionally, a sparse set of features and points was extracted from the imaging data to mimic realistic intraoperative digitization using standard methods (e.g. tracked ultrasound and surface fiducials). With digitization data completely realized with varying levels of density, registration methods were evaluated and compared. In particular, rigid and sparse-data non-rigid registration methods were compared

to the ‘best’ comparator which was a symmetric diffeomorphic image-to-image registration algorithm with B-spline regularization available in the Advanced Normalization Tools (ANTs) repository[14]. This image registration deformation field was then used to analyze volume change and anisotropy for the entire breast and for adipose and glandular tissue independently to better understand the underlying biomechanics associated with breast deformations. Important findings on the fidelity of sparse-data-driven approaches as well as future directions in development are reported, and this information could be used to inform future registration techniques for BCS.

2. METHODS

2.1 Image Acquisition and Preprocessing

Supine breast MR imaging was performed on the left and right breasts of seven healthy volunteers using a Phillips 3T closed bore scanner and a 16-channel torso coil. Volunteers were enrolled with informed consent in a study approved by the Institutional Review Board at Vanderbilt University. T1 High Resolution Isotropic Volume Excitation (THRIVE) sequence scans were obtained with one of two voxel sizes ($0.357\times0.357\times1$ mm^3 or $0.391\times0.391\times1$ mm^3) with the ipsilateral arm down by the torso to mimic preoperative positioning and with the ipsilateral arm up by the head to mimic intraoperative positioning. Twenty-six MR visible fiducials were placed on the surface of each breast prior to imaging. Three out of the fourteen breast images were omitted due to large imaging artifacts leaving eleven (n=11) breasts from seven individuals included in the study.

3D breast volumes were manually segmented from the MR images along the boundary between the chest wall and breast parenchyma. The surface fiducial markers were manually labeled and used as corresponding points in the mock preoperative and intraoperative positions. For each volunteer, 18–26 corresponding subsurface features were manually picked in the mock preoperative and intraoperative images for ‘gold standard’ target evaluation.

2.2 Registration Methods

Three registration methods were evaluated. The first method consisted of a rigid registration calculated from the surface fiducials using a conventional least-squares singular value decomposition point based registration method[15]. The second method utilized a nonrigid FEM-based registration performed based on the methodology proposed in Heiselman et al.[16]. Briefly, 45 control points were placed on the surface of the preoperative 3D breast mesh excluding the skin surface and individually perturbed in the x, y, and z directions to create a basis of displacement modes which were solved as forward homogeneous isotropic elastic boundary value problems with Young’s Modulus E = 2100 Pa and Poisson ratio ν = 0.45. Levenberg-Marquardt optimization was used to solve for the linear combination of these modes that minimized the distances between the deformed and intraoperative MR-visible skin fiducials, intra-fiducial skin surface, and sparsely sampled chest wall surface while also incorporating a strain energy penalty to reduce unrealistic deformations. This optimization is represented in the equation,

$$\Omega(\boldsymbol{\beta}) = \sum_F \frac{\omega_F}{N_F} \sum_{i=1}^{N_F} f_i^2 + \omega_E {f_E}^2 \quad (1)$$

where $\Omega(\boldsymbol{\beta})$ is the objective function, $\boldsymbol{\beta}$ is the parameter vector representing the linear combination of displacement modes plus a rigid translation and rotation, f_i is the error between the deformed and intraoperative point i, N_F is the number of points within a feature F, ω_F is the weight of the feature F, f_E is the strain energy of the deformation, and ω_E is the strain energy weight which was set to 10^{-9} Pa^{-2}. In this registration, three data features —the MR-visible skin fiducial points, the intra-fiducial skin surface point cloud, and the sparsely sampled chest wall surface point cloud—were included in the objective function to optimize the registration parameter vector $\boldsymbol{\beta}$. It should be noted that in this framework, sparse chest wall surface sampling represents equivalent data that would be acquired using tracked ultrasound imaging demonstrated in previous work[9,11].

The third method was a 3D image-to-image registration. This approach registered the preoperative and intraoperative images using a symmetric diffeomorphic image registration algorithm with explicit B-spline regularization available in the ANTs repository[14]. Images were masked using a dilated breast volume segmentation mask so that the MR visible fiducials were included in the masked volume. The registration was initialized with the rigid point based registration method, i.e. the initial comparator in this study, and followed by the deformable b-spline symmetric normalization method. The optimal parameters used for ANTs registration are reported in Table 1.

2.3 Evaluation of Registration Accuracy

The resulting deformations were applied to the preoperative skin fiducials and subsurface targets and compared to their true intraoperative locations. To evaluate registration accuracy at the skin surface, fiducial registration error ($\overline{\text{FRE}}$) was calculated as the root mean squared error between corresponding fiducial points,

$$\overline{\text{FRE}} = \sqrt{\frac{1}{N} \sum_{i=1}^{N} FRE_i^2} \quad (2)$$

where FRE_i is the distance between the deformed i^{th} fiducial and the corresponding i^{th} intraoperative fiducial. Similarly, target registration error ($\overline{\text{TRE}}$) was calculated as the root mean squared error between targets,

$$\overline{\text{TRE}} = \sqrt{\frac{1}{N} \sum_{i=1}^{N} TRE_i^2} \quad (3)$$

where TRE_i is the distance between the deformed i^{th} target and the corresponding intraoperative i^{th} target. $\overline{\text{FRE}}$s and $\overline{\text{TRE}}$s were compared across registration methods using paired t-tests ($\alpha = 0.05$).

2.4 Tissue Characterization

Mechanics-based metrics representing volume change and directional preference in volume change were calculated as a means of interpreting the ANTs 'best comparator' deformation field as described in Amelon et al.[17]. The Jacobian determinant (J) to measure volume change and the Anisotropic Deformation Index (ADI) to measure anisotropy were computed using the following formulas,

$$J = \lambda_1\lambda_2\lambda_3 \quad ADI = \sqrt{\left(\frac{\lambda_1 - \lambda_2}{\lambda_2}\right)^2 + \left(\frac{\lambda_2 - \lambda_3}{\lambda_3}\right)^2} \tag{4}$$

where λ are the eigenvalues, or the principal stretches, of the deformation gradient tensor with $\lambda_1 > \lambda_2 > \lambda_3$ for material that has anisotropic behavior in all 3 principal directions and $\lambda_1 = \lambda_2 = \lambda_3$ for isotropic materials. J<1 indicates volume contraction, J=1 indicates no volume change, and J>1 indicates volume expansion. ADI=0 indicates isotropic deformation and ADI>0 indicates increasingly anisotropic deformation[17]. J and ADI were calculated at every element in the breast mesh using the data provided by the ANTs deformation field. The metrics were averaged within semi-manually segmented adipose tissue and within semi-manually segmented glandular tissue. Average metrics were compared across tissue types using paired t-tests ($\alpha = 0.05$).

3. RESULTS

Figure 1 (*top row*) illustrates an example from one volunteer of the data utilized for the various registration methods employed in this work. The MR-visible skin fiducials (blue) were used for rigid registration, the skin fiducials combined with the intra-fiducial skin surface point cloud (yellow) and the sparsely sampled chest wall surface (red) were used for the nonrigid model-based registration, and the 3D image volume was used for ANTs registration. Figure 1 (*bottom row*) shows sample registrations from each registration method with increasingly better target alignment.

The distribution of FREs for each registration method is shown in Figure 2A. The average of the root mean squared error FRE values across all breasts was 7.8 ± 1.7, 2.5 ± 1.1, and 3.1 ± 1.1 mm for the rigid, model-based nonrigid, and ANTs registration methods respectively (mean ± standard deviation). When compared to rigid registration, nonrigid model-based registration resulted in a 68% improvement in FRE ($p<0.001$) and ANTs resulted in a 60% improvement in FRE ($p<0.001$). There was no significant difference in FRE between the nonrigid model-based registration and the ANTs registration ($p=0.22$).

The distribution of TREs for each registration method is shown in Figure 2B. The average of the root mean squared error TRE values across all breasts was 10.4 ± 2.3, 6.4 ± 1.5, and 2.8 ± 1.3 mm for the rigid, model-based nonrigid, and ANTs registration methods respectively (mean ± standard deviation). When compared to rigid registration, nonrigid model-based registration resulted in a 38% improvement in TRE ($p<0.001$) and ANTs resulted in a 73% improvement in TRE ($p<0.001$). ANTs registration improved TRE by 56% compared to nonrigid model-based registration ($p<0.001$).

The average J and ADI index values computed from the ANTs deformation field and stratified by tissue type are reported in Table 2. The average J value for adipose tissue was 0.96 ± 0.02 across all cases (mean ± standard deviation). Comparatively, the average J value for glandular tissue was 1.01 ± 0.02, which was significantly higher than adipose tissue ($p<0.001$). This indicates that on average, ANTs predicted slight relative contraction of adipose tissue and expansion of glandular tissue during the deformation from arm-down to arm-up positions. The average ADI value for adipose tissue was 0.54 ± 0.09 across all cases, and the average ADI value for glandular tissue was 0.60 ± 0.15 (mean ± standard deviation). There was no significant difference in ADI value between adipose and glandular tissue ($p=0.23$). This suggests that ANTs registration predicts both tissue types to have similar anisotropic behavior.

4. DISCUSSION

This comparison of three registration methods demonstrated significant improvement with increasing method complexity and data extent. The nonrigid model-based registration method performed significantly better than the rigid registration method in both FRE and TRE, which is consistent with the fact that there are large nonrigid deformations that occur between arm-down to arm-up positions[9]. This suggests that a BCS image guidance system would benefit from nonrigid registration to better localize subsurface breast tumors. However, the nonrigid model-based registration performance was limited, and possible explanations for this may be the need for additional geometric data, the lack of heterogeneity in the model, or the lack of anatomic structural components in the model such as the suspensory Cooper's ligaments of the breast[18]. Additionally, the ANTs 3D image registration method performed significantly better than both the rigid and nonrigid model-based registration methods when considering TRE and significantly better than the rigid registration when considering FRE. This difference is expected given that ANTs registration is intensity-based and utilizes dense image volume data with voxel-to-voxel matching of image intensity features, while the nonrigid model-based registration is driven with sparse point-cloud data consistent with the limitations and practices of standard surgical suites. The nonrigid model-based registration method used between 840 – 1,110 data points when combining the MR-visible skin fiducials, intra-fiducial skin surface point cloud, and sparsely sampled chest wall surface point cloud while the ANTs registration method used over 1 million voxels depending on dimensions of the masked image volume. While it is unlikely that any nonrigid sparse-data registration method could outperform ANTs given the discrepancy in the amount of input data in this experiment, it is interesting to consider the workflow of the procedure in the context of these registrations. Given the encumbrance of intraoperative MR imaging data, its practical use for procedural updates is compromised. The reduced data acquisition requirement of the model-based approach enables an easier translational pathway and could allow for a more continuous registration update that could potentially result in superior performance despite being less accurate in idealized tests.

Another contribution of this work is the utilization of the ANTs registration package for breast MR supine-to-supine image registration. While ANTs registration has been used extensively on neuroimaging data, its application for breast imaging registration is more limited. The ANTs symmetric image normalization (SyN) method with explicit B-

spline regularization (a directly manipulated free-form deformation algorithm) that used cross correlation as the similarity metric outperformed ANTs registrations with other parameters such as Gaussian smoothing regularization and mutual information similarity metric. This behavior likely arises because B-spline regularization can better capture the large deformations present in the breast. Other diffeomorphic image registration packages and algorithms have been applied to breast images previously including Elastix, Thirion's demons algorithm, and the DRAMMS algorithm[19,20]. While more analysis is needed to evaluate ANTs registration performance compared to other available image registration packages, the ANTs registration parameters reported here may be applicable for additional breast image registration applications including longitudinal studies, inter-subject comparisons when studying tumor treatment responses, and performing multimodal registrations[21,22].

Overall, the average J index value across all cases was 0.97 ± 0.02 suggesting, as expected, nearly no volume change (J=1) in breast tissue between arm-down and arm-up positioning. However, examining the average J index within adipose and glandular tissue types separately showed significant differences. The J index for glandular tissue was slightly higher than the J index for adipose tissue. This suggests a variable response to different arm positions between adipose and glandular tissue, with glandular tissue expanding slightly more than adipose tissue. Additionally, the average ADI index value across all cases was 0.53 ± 0.09 suggesting that the breast undergoes anisotropic deformation (ADI>0) between arm-down and arm-up positions. Both J and ADI index differences imply that nonrigid modeling methods may benefit from incorporating material properties reflecting heterogeneity and anisotropy.

With respect to limitations, all conclusions drawn from the biomechanical indices assume that the ANTs deformation field is correctly representing the true local deformation field that occurs between arm-down and arm-up positioning. It is important to note that the ANTs deformation field is subject to method-specific bias from the image-to-image registration algorithm. The TRE results show that the ANTs registration is more accurate than rigid and nonrigid model-based registration and achieves a registration accuracy lower than 4 mm for 75% of targets in all volunteers. However, the average maximum target registration error across all cases is 8.9 mm for ANTs registration, with the error from an individual target from one case being as high as 20.8 mm. This implies that there are some regions of the image volumes where ANTs registration is not accurate. This may be because of poor image quality in those regions, MRI image artifacts, or a lack of distinguishable image features. These inaccuracies should be considered when using the biomechanical indices to make inferences about tissue properties.

5. CONCLUSION

This work evaluated three registration methods – rigid, a nonrigid model-based method, and an ANTs 3D image diffeomorphic method – for registering arm-down to arm-up supine breast MR images on eleven healthy volunteer breast cases while also providing an analysis of breast tissue biomechanical properties based on the image registration deformation field. On average, nonrigid model-based registration driven with sparse data localized subsurface

target points with 6.4 ± 1.5 mm TRE, which was 38% better than rigid registration and compatible with real time registration goals for lumpectomy. In contrast, although not practical intraoperatively, ANTs localized subsurface points with 2.8 ± 1.3 mm TRE when driven with full volumetric images and was 73% better than rigid registration. The FRE also significantly improved when comparing rigid to nonrigid model-based registration and when comparing rigid to ANTs registration, although there was no significant difference in FRE between the nonrigid model-based and ANTs registration. Biomechanical indices calculated from the ANTs deformation field suggest that adipose and glandular tissue vary in terms of volume change and that the breast undergoes anisotropic deformation during the arm-down to arm-up motion. This investigation into supine breast image registration lays the groundwork for future model-based registration methods for surgical guidance systems that rely on accurate registration for intraoperative tumor localization during lumpectomy procedures.

ACKNOWLEDGEMENTS

This work has been supported by the NIH grants R01EB027498 and T32EB021937 and NSF-GRFP.

REFERENCES

[1]. Waljee JF, Hu ES, Newman LA and Alderman AK, “Predictors of Re-excision among Women Undergoing Breast-Conserving Surgery for Cancer,” Ann. Surg. Oncol 2008 155 15(5), 1297–1303 (2008). [PubMed: 18259820]

[2]. Mann RM, Cho N and Moy L, “Breast MRI: State of the Art,” 10.1148/radiol.2019182947 292(3), 520–536 (2019).

[3]. Nakamura R, Nagashima T, Sakakibara M, Sangai T, Fujimoto H, Arai M, Shida T, Kaneoya K, Ueda T, Nakatani Y, Hashimoto H and Miyazaki M, “Breast-conserving surgery using supine magnetic resonance imaging in breast cancer patients receiving neoadjuvant chemotherapy,” The Breast 17(3), 245–251 (2008). [PubMed: 18024036]

[4]. Pallone MJ, Poplack SP, Avutu HBR, Paulsen KD and Barth RJ, “Supine breast MRI and 3D optical scanning: A novel approach to improve tumor localization for breast conserving surgery,” Ann. Surg. Oncol 21(7), 2203–2208 (2014). [PubMed: 24619494]

[5]. Alderliesten T, Loo C, Paape A, Muller S, Rutgers E, Peeters M-JV and Gilhuijs K, “On the feasibility of MRI-guided navigation to demarcate breast cancer for breast-conserving surgery,” Med. Phys 37(6), 2617–2626 (2010). [PubMed: 20632573]

[6]. Mallory MA, Sagara Y, Aydogan F, DeSantis S, Jayender J, Caragacianu D, Gombos E, Vosburgh KG, Jolesz FA and Golshan M, “Feasibility of Intraoperative Breast MRI and the Role of Prone Versus Supine Positioning in Surgical Planning for Breast Conserving Surgery,” Breast J. 23(6), 713 (2017). [PubMed: 28295903]

[7]. Alam F, Rahman SU, Ullah S and Gulati K, “Medical image registration in image guided surgery: Issues, challenges and research opportunities,” Biocybern. Biomed. Eng 38(1), 71–89 (2018).

[8]. Gombos EC, Jayender J, Richman DM, Caragacianu DL, Mallory MA, Jolesz FA and Golshan M, “Intraoperative supine breast MR imaging to quantify tumor deformation and detection of residual breast cancer: Preliminary results,” Radiology 281(3), 720–729 (2016). [PubMed: 27332738]

[9]. Richey WL, Heiselman JS, Luo M, Meszoely IM and Miga MI, “Impact of deformation on a supine-positioned image guided breast surgery approach,” Int. J. Comput. Assist. Radiol. Surgery (2021).

[10]. Ebrahimi M, Siegler P, Modhafar A, Holloway CMB, Plewes DB and Martel AL, “Using surface markers for MRI guided breast conserving surgery: A feasibility survey,” Phys. Med. Biol 59(7), 1589–1605 (2014). [PubMed: 24614540]

[11]. Conley RH, Meszoely IM, Weis JA, Pheiffer TS, Arlinghaus LR, Yankeelov TE and Miga MI, “Realization of a biomechanical model-assisted image guidance system for breast cancer surgery using supine MRI,” Int. J. Comput. Assist. Radiol. Surg 10(12), 1985 (2015). [PubMed: 26092657]

[12]. Eder M, Raith S, Jalali J, Volf A, Settles M, Machens HG and Kovacs L, “Comparison of different material models to simulate 3-D breast deformations using finite element analysis,” Ann. Biomed. Eng 42(4), 843–857 (2014). [PubMed: 24346816]

[13]. McGhee DE and Steele JR, “Breast biomechanics: What do we really know?,” Physiology 35(2), 144–156 (2020). [PubMed: 32027563]

[14]. Tustison NJ and Avants BB, “Explicit B-spline regularization in diffeomorphic image registration,” Front. Neuroinform 7(39) (2013).

[15]. Arun KS, Huang TS and Blostein SD, “Least-squares fitting of two 3-d point sets,” IEEE Trans. Pattern Anal. Mach. Intell 9(5), 698–700 (1987). [PubMed: 21869429]

[16]. Heiselman JS, Jarnagin WR and Miga MI, “Intraoperative Correction of Liver Deformation Using Sparse Surface and Vascular Features via Linearized Iterative Boundary Reconstruction,” IEEE Trans. Med. Imaging 39(6), 2223–2234 (2020). [PubMed: 31976882]

[17]. Amelon R, Cao K, Ding K, Christensen GE, Reinhardt JM and Raghavan ML, “Three dimensional characterization of regional lung deformation,” J. Biomech 44(13), 2489–2495 (2011). [PubMed: 21802086]

[18]. Rajagopal V, Nielsen PMF and Nash MP, “Modeling breast biomechanics for multi-modal image analysis—successes and challenges,” Wiley Interdiscip. Rev. Syst. Biol. Med 2(3), 293–304 (2010). [PubMed: 20836030]

[19]. Mehrabian H, Richmond L, Lu Y and Martel AL, “Deformable Registration for Longitudinal Breast MRI Screening,” J. Digit. Imaging 31(5), 718 (2018). [PubMed: 29654424]

[20]. Ou Y, Weinstein SP, Conant EF, Englander S, Da X, Gaonkar B, Hsieh M-K, Rosen M, Demichele A, Davatzikos C and Kontos D, “Deformable Registration for Quantifying Longitudinal Tumor Changes During Neoadjuvant Chemotherapy,” Magn. Reson. Med 73, 2343–2356 (2015). [PubMed: 25046843]

[21]. Li X, Dawant BM, Brian Welch E, Bapsi Chakravarthy A, Freehardt D, Mayer I, Kelley M, Meszoely I, Gore JC and Yankeelov TE, “A Nonrigid Registration Algorithm for Longitudinal Breast MR Images and the Analysis of Breast Tumor Response,” Magn Reson Imaging 27(9), 1258–1270 (2009). [PubMed: 19525078]

[22]. Guo Y, Sivaramakrishna R, Lu C-C, Suri JS and Laxminarayan S, “Breast image registration techniques: a survey,” Med. Biol. Eng. Comput 2006 441 44(1), 15–26 (2006). [PubMed: 16929917]

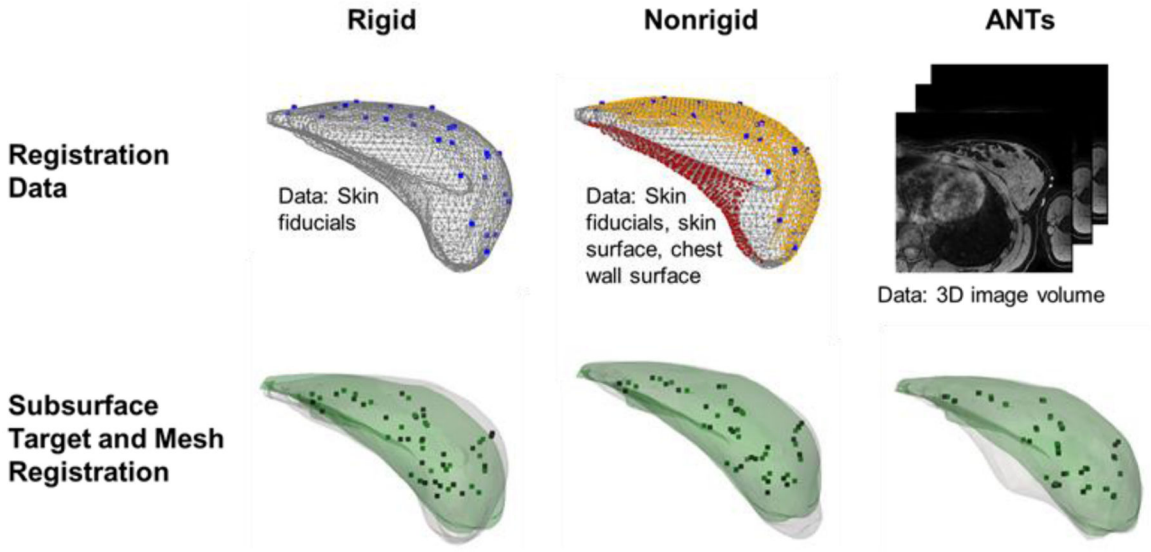

Figure 1:

The process for rigid (left), nonrigid (middle), and ANTs (right) registrations shown on axial views of a segmented breast mesh. In the top row, the data utilized for each registration is visualized. Rigid registration used MR-visible skin fiducials (blue), nonrigid model-based registration used MR-visible skin fiducials (blue), skin surface (yellow), and chest wall surface (red), and ANTs registration used the 3D image volume. In the bottom row, the registered mesh (gray) and targets (black) are overlaid on the ground truth arm-up mesh and targets shown in green.

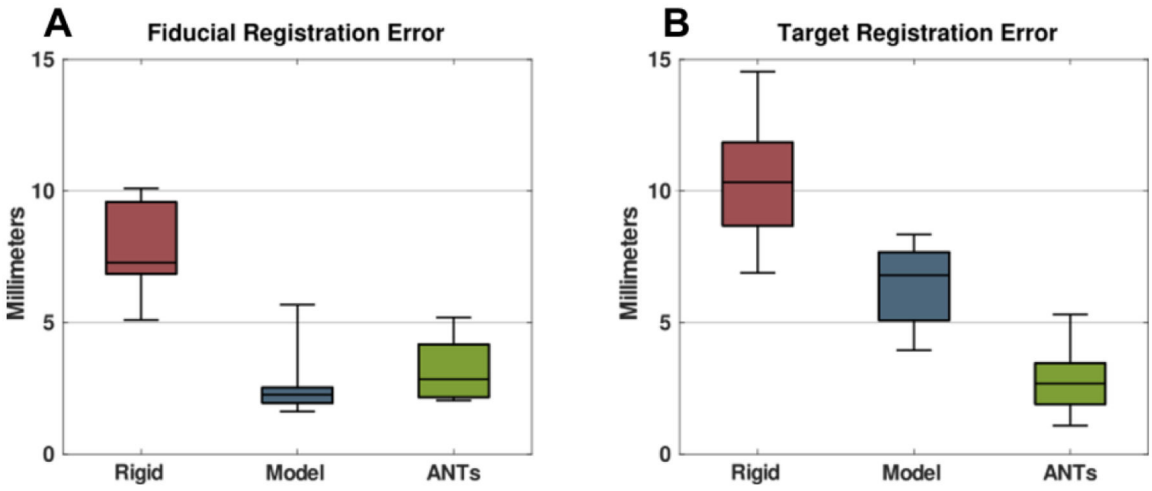

Figure 2:

Registration methods performance comparison showing (A) fiducial registration error ($\overline{\text{FRE}}$) and (B) target registration error ($\overline{\text{TRE}}$) from 11 breasts. Whiskers represent minimum and maximum FRE and TRE values.

Table 1:

ANTs registration parameters used for optimal breast MR image registration.

ANTs Registration Parameters	
ANTs Script	antsRegistrationSyN.sh
Initialization	Rigid point based registration
Stages	Deformable b-spline symmetric normalization
Similarity metric	Cross correlation
Histogram bins	32
Histogram matching	Yes
Spline distance	26
Gradient step size	0.1

Table 2:

Average J and ADI indices reported by tissue type.

	Adipose (mean ± standard deviation)	**Glandular (mean ± standard deviation)**	**Significance**
J	0.96 ± 0.02	1.01 ± 0.02	Yes ($p<0.001$)
ADI	0.54 ± 0.09	0.60 ± 0.15	No ($p=0.23$)